Organic chemistry of NH_3 and HCN induced by an atmospheric abnormal glow discharge in N_2-CH_4 mixtures

EPJ AP

Applied Physics

EPJ.org
your physics journal

Eur. Phys. J. Appl. Phys. **53**, 11001 (2011) DOI: 10.1051/epjap/2010100191

Organic chemistry of NH_3 and HCN induced by an atmospheric abnormal glow discharge in N_2-CH_4 mixtures

G. Horvath, F. Krcma, L. Polachova, K. Klohnova, N.J. Mason, M. Zahoran and S. Matejcik

EDP SCIENCES

The title "The European Physical Journal" is a joint property of EDP Sciences, Società Italiana di Fisica (SIF) and Springer

Eur. Phys. J. Appl. Phys. **53**, 11001 (2011)
DOI: 10.1051/epjap/2010100191

THE EUROPEAN PHYSICAL JOURNAL APPLIED PHYSICS

Regular Article

Organic chemistry of NH_3 and HCN induced by an atmospheric abnormal glow discharge in N_2-CH_4 mixtures

G. Horvath[1,2,a], F. Krcma[3], L. Polachova[2,3], K. Klohnova[3], N.J. Mason[2], M. Zahoran[1], and S. Matejcik[1]

[1] Department of Experimental Physics, Comenius University, Mlynska dolina F2, 84248 Bratislava, Slovakia
[2] Department of Physics and Astronomy, The Open University, Walton Hall, MK7 6AA, Milton Keynes, UK
[3] Brno University of Technology, Faculty of Chemistry, Purkynova 118, 61200 Brno, Czech Republic

Received: 10 May 2010 / Accepted: 7 October 2010
Published online: 23 December 2010 –

Abstract. The formation of the chemical products produced in an atmospheric glow discharge fed by a N_2-CH_4 gas mixture has been studied using Fourier Transform InfraRed (FTIR) and Optical Emission Spectrometry (OES). The measurements were carried out in a flowing regime at ambient temperature and pressure with CH_4 concentrations ranging from 0.5% to 2%. In the recorded emission spectra the lines of the second positive system CN system and the first negative system of N_2 were found to be the most intensive but atomic H^{α}, H^{β}, and C (247 nm) lines were also observed. FTIR-measurements revealed HCN and NH_3 to be the major products of the plasma with traces of C_2H_2. These same molecules have been detected in Titan's atmosphere and the present experiments may provide some novel insights into the chemical and physical mechanisms prevalent in Titan's atmosphere with these smaller species believed to be the precursors of heavier organic species in Titan's atmosphere and on its surface.

1 Introduction

The Cassini space mission to Saturn and the release of its Huygens probe onto its largest moon, Titan, has led to a wealth of data on the atmospheric and surface composition of Titan, presenting us with a set of unexpected results including the observation of hydrocarbon lakes – the first liquid "seas" on a solar system body outside the earth – and the observation of anions in the upper atmosphere (ionosphere) [1]. In order to understand the physical and chemical processes leading to such observed phenomena laboratory simulations are required.

The dense atmosphere of Titan is mostly composed of N_2 with a few percent of CH_4. The most important minor compounds detected by Cassini-Huygens are nitriles (HCN, HC_3N, HC_5N, C_2N_2) believed to be formed by as a result of dissociation of nitrogen and methane either by solar induced photolysis or by electron impact [2] and hydrocarbons (C_2H_2, C_2H_4, C_2H_6, C_3H_8, C_3H_4 [2]). The presence of clouds and strong convective motions are a particular feature of Titan's lower atmosphere. Charged particles, originating from the Saturnian magnetosphere, can accumulate on droplets within the clouds of the troposphere. Neutralization of these charged particles leads to corona discharges within the clouds which can induce chemical reactions in the troposphere [2].

There have been several theoretical models of Titan's atmosphere many of which considered three-body electron attachment to radicals or collisional charging of aerosols as the source of negatively charged species [3,4]. Probably because the first process is negligible at high altitude (densities lower than 10^{15} cm^{-3}) and because aerosols were not expected to be present above ∼500 km, the presence of negative ions in Titan's upper atmosphere had not postulated before the Cassini-Huygens mission. Therefore, the detection of negative ions in Titan's upper atmosphere [5,6] has lead to new models of the chemistry in Titan's upper atmosphere [1,7].

However such models need to be tested against laboratory mimics. Discharges have been shown to be good mimics of planetary atmospheres providing insights into both physical and chemical processes of such atmospheres. DBD, glow, microwave, RF and corona discharges [8–19], have all been used in order to study electron-molecule and ion-molecule reactions in planetary atmospheres. Since methane is the primary species in Titan's atmosphere whose dissociation leads to further reactive chemistry it is valuable to review studies on methane in discharges.

Methane conversion has been studied using gliding arc plasma [20]. In this work, conducted at atmospheric pressure, four kinds of additive gases – He, Ar, N_2 and CO_2 – with admixture concentrations in the range from 0 to 80%, were used to investigate their effects on methane conversion. Methane conversion was increased with the increasing concentration of helium, argon, and nitrogen in the feed gas but decreased as the CO_2 concentration increased. H_2 and C_2H_2 were the major products of such discharges.

[a] e-mail: horeszka@gmail.com

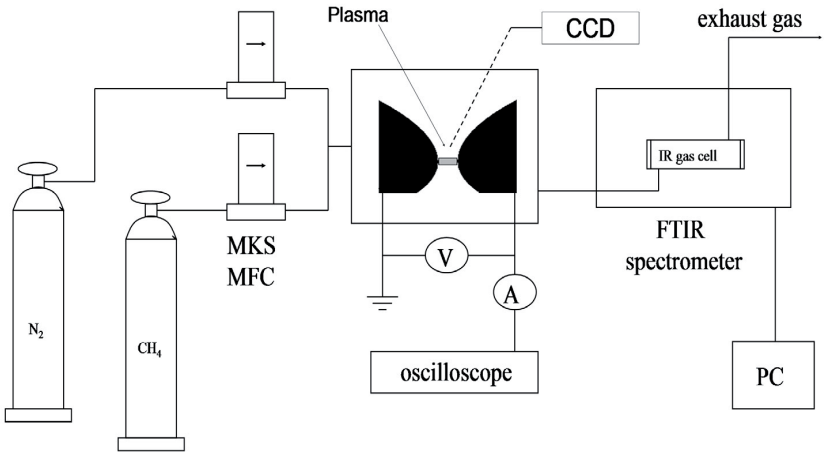

Fig. 1. Schematic diagram of the experimental apparatus used for FTIR and OES analysis of gaseous products produced in a gliding arc discharge fed by various mixtures of methane in nitrogen.

Non-oxidative methane coupling in hybrid plasma-catalytic reactors has been studied by Młotek et al. [21]. A combination of a gliding arc discharge and a packed bed of catalyst pellets revealed high efficiency methane conversion. Two catalysts made of Pt and Pd supported by alumina ceramics were prepared and tested. The methane conversion was investigated in two gliding discharge reactors supplied by 1-phase or 3-phase circuits (50 Hz). The most dominant species formed in these discharges was acetylene but the formation of other non-volatile products was also observed. In the presence of catalysts soot formation was strongly reduced. Owing to these catalysts, ethylene and ethane became the main gaseous products replacing acetylene.

In this paper we report the results of a new investigation of the organic chemistry prevalent in an atmospheric glow discharge fed by a N_2-CH_4 gas mixture with CH_4 contents in the range of 0.5% to 2%.

2 Experimental set-up

The apparatus used in these experiments is shown schematically in Figure 1. The reactor was connected to the long path IR gas cell equipped with KCl windows and placed in a Nicolet Nexus FTIR spectrometer. Optical Emission Spectrometry (OES) using a Jobin Yvon Triax 550 spectrometer with a CCD detector was used to monitor the optical emission from the N_2/CH_4 plasma. The spectral response of this spectrometer was obtained using an Oriel radiation standard lamp. The 3600 g/mm grating was used for the rotationally resolved CN violet 0–0 band acquisition, all other spectra were measured with 1200 g/mm grating. The flow rates through the reactor for both CH_4 (purity 99.995%) and N_2 (purity 99.999%) were regulated using MKS mass flow controllers. All measurements were carried out within a flowing regime with a total flow rate of 200 sccm. The discharge electrode system had the standard configuration of a classical gliding arc, a pair of stainless steel holders positioned in parallel to the iron electrodes but in this case the plasma was not gliding due to the low flow rate and therefore stable abnormal glow plasma occurred between the electrodes at their shortest distance of 2 mm, thus forming a plasma channel with a diameter of 1 mm. With increasing current (15–40 mA) the voltage was slightly decreasing from 400 V to 350 V. Electrical parameters were measured using a Tektronix oscilloscope with a high voltage probe and 10 Ω resistor for current measurement.

The reactor chamber had a volume of 0.3 L. The discharge was powered by a home-made DC HV source. All the experiments were carried out at atmospheric pressure and at ambient temperatures. The discharge was typically operated for between 60 and 120 min during which time the nascent reactor temperature (as measured by thermocouples on the reactor walls) did not rise above 320 K. Experiments were performed for different N_2:CH_4 ratios in the range from 0.5% to 2% CH_4 in N_2. A pure CH_4/N_2 gas mixture without plasma was measured as the background spectra for FTIR measurements.

The discharge power was calculated using the formula:

$$P = UI, \tag{1a}$$

where U is the voltage drop across the electrodes and I is the discharge current.

The specific input energy was calculated using the formula:

$$\eta = \frac{P}{Q} \quad \text{(kJ/L)}, \tag{1b}$$

where P is the power calculated using equation (1a) and Q is the flow rate. The estimated values were 1.8 kJ/L for the lowest current $I = 15$ mA and 4.2 kJ/L for the highest current $I = 40$ mA used in our experiments.

The gaseous product concentrations were calculated using the Beer-Lambert formula (2) using IR absorption cross section data found in the HITRAN* database [22]:

$$A = n\, l\, \sigma, \tag{2}$$

where A is the absorbance measured experimentally, n (cm^{-3}) is the concentration of detected compound,

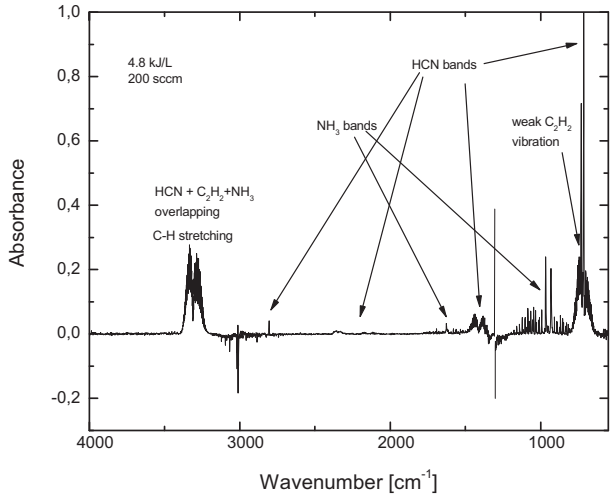

Fig. 2. A typical FTIR spectrum recorded in a gas cell filled with products formed in the discharge reactor fed by a CH_4-N_2 gas mixture with a 2:98 ratio, operated at atmospheric pressure and a total gas flow 200 sccm. The unit energy has a value of 4.8 kJ/L. Note the negative absorbance indicates the conversion of CH_4 during the operation of the discharge.

l (cm) is the length of the absorption path in IR cell and σ (cm^2) is the IR absorption cross-section.

3 Experimental results

3.1 FTIR analysis of final gaseous products

A typical FTIR spectrum revealing the products formed in the discharge fed by 2% CH_4 in N_2 is shown in Figure 2. Similar spectra were observed for other CH_4/N_2 molar ratios. Using the HITRAN spectral data individual absorption features can be assigned to specific compounds. Besides the remaining CH_4 (3230–2704 cm^{-1}; 1408–1169 cm^{-1}) obvious infrared spectra absorption bands of C≡C were observed at the wave numbers 3386–3217 cm^{-1} which is the typical C-H stretching band of hydrogen cyanide HCN and acetylene C_2H_2. The strongest feature, at 713 cm^{-1}, is due to HCN, the weak peak at 729 cm^{-1} is due to C_2H_2. However, we found no features corresponding to C_2H_4 (which has a well known band between 800–1100 cm^{-1}, maximum at 956 cm^{-1} and a band between 3000–3200 cm^{-1}, maximum at 3138 cm^{-1}). In contrast to our earlier measurements made in a coaxial corona discharge [23], NH_3 was observed as a new product in the abnormal glow discharge identified by its strong peak at 966 cm^{-1}, surrounded by dense rotational in range 800–1200. Bands at around 3300 cm^{-1} were composed of overlapping bands from HCN, NH_3 and C_2H_2.

From the measured absorbance values the concentrations of individual compounds were calculated using the Beer-Lambert formula with molecular IR absorption cross-section data being taken from the HITRAN spectral database. The dependence of the concentration NH_3 and HCN on the gas flow rate are shown in Figures 3a–3d. C_2H_2, as the minor product, did not exceed concentrations of 100 ppm during the measurements and was found to slightly decrease with increasing power. It should be noted that diatomic molecules such as H_2 can not be detected using FTIR.

The generation of energetic electrons has been recognized as the initial step in all the reactions in the plasma region, in particular inelastic collisions of methane molecules with energetic electrons leads to the formation of some active free radicals such as C, CH, CH_2 and CH_3.

It is evident that the product formation is accompanied by a decrease in concentration of CH_4 but because of the overlap of CH_2 and CH_3 stretching bands in CH_4 region we can not determine the degree of its decomposition from the measured changes of absorbance in the derivative spectra.

As shown in Figure 3, the discharge current I has a significant effect on both the synthesis of HCN and NH_3. The larger the value of I, the more HCN and NH_3 are formed. It should also be noted that the yields of HCN increase with increasing initial CH_4 content whilst the yield of NH_3 decreases as the concentration of CH_4 increases.

3.2 Optical Emission Spectroscopy of the glow region

Optical Emission Spectroscopy (OES) is a common technique used to investigate glow discharges since it produces no perturbation in the plasma. The basic premise of this technique is that the intensity of the light emitted at particular wavelengths from an excited state is proportional to the density of species in that excited state [24]. Therefore measurement of intensities provides a method for measuring the rotational, vibrational temperatures of the plasma species (T_r, T_v) the electron temperature (T_{ve}) and the relative concentration of species, which can be converted into an absolute concentration if we know the Electron Energy Distribution Function (EEDF) and energy dependent cross sections for the electron impact excitation processes [24,25]. Unfortunately, in our case the plasma was not in local thermodynamical equilibrium (LTE), thus the molecules do not exhibit a Maxwell-Boltzmann distribution and determination of their absolute concentrations from the spectra was not possible. However, the measurements of the intensities of selected emission lines and bands (Fig. 5) provide a measure of the relative concentration of species as a function of discharge current.

The spectra were recorded integrally over whole plasma volume. A selected part of a typical emission spectrum is shown in Figure 4. As expected N_2 and CN bands were the most dominant. The spectra were composed of the following molecular spectral systems: the second positive system of neutral N_2 ($C^3\Pi_u \rightarrow B^3\Pi_g$), the first negative system of N_2^+ ion ($B^2\Sigma_u^+ \rightarrow X^2\Sigma_g^+$), the CN violet ($B^2\Sigma^+ \rightarrow X^2\Sigma^+$a) and red systems ($A^2\Sigma^+ \rightarrow X^2\Sigma^+$) and the C_2 Swan bands. Besides these the strong atomic H^α line, weaker H^β line and weak lines of C (247 nm – measured in the second order) and N^+ (399.5 nm) were detected.

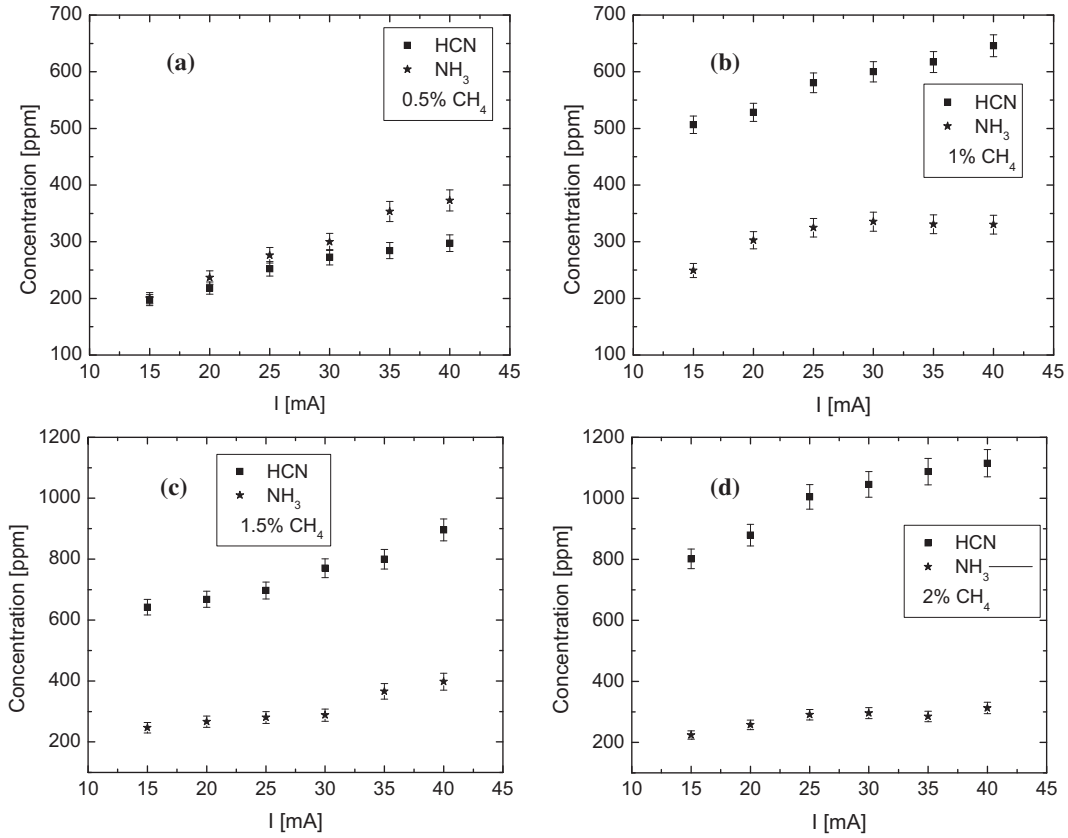

Fig. 3. The dependence of HCN and NH_3 concentrations on the discharge current for different initial CH_4 concentrations ((a) 0.5, (b) 1, (c) 1.5 and (d) 2%) in N_2 plasma.

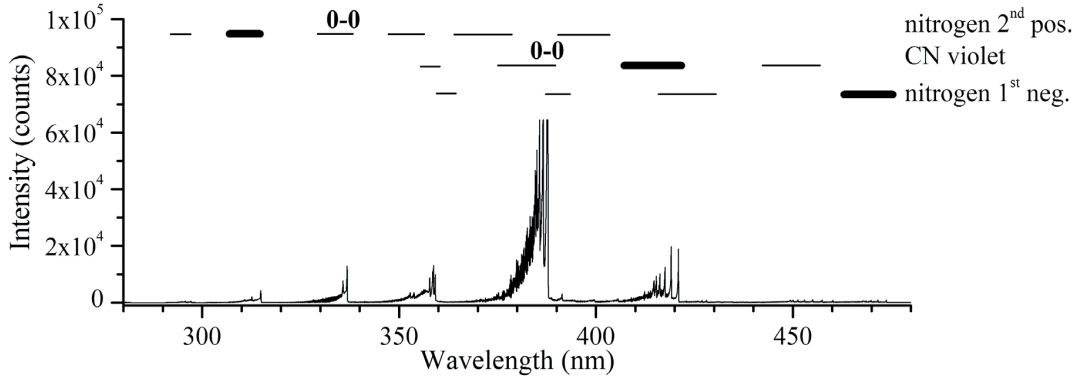

Fig. 4. A portion of the emission spectrum recorded using a discharge current of 40 mA and 2.0% CH_4 content in N_2. Components of several emission bands are labeled.

The relative emission intensities for the selected emission bands are shown in Figure 5. The variation of the intensity ratio $I(N_2^+)/I(N^*_{2(1-0)})$ with discharge current suggests a slightly increased occurrence of N_2^+ ions in comparison with N_2^* molecules. These results may be explained by N_2^+ emission being more sensitive to high-energy electrons than N_2^* due to the higher excitation threshold energy compared with N_2^*. This suggests that the degree of ionization of the plasma increases with the number of free electrons. On the other hand this small increase in $I(N_2^+)/I(N^*_{2(1-0)})$ intensity ratio indicates that any increase in the electron energy distribution is also small and the increasing temperature T_g is due to the increasing concentration of electrons.

The high emission intensity of C_2 Swan system suggests a high degree of decomposition of CH_4 into C then C_2 radicals which is confirmed by the absence of emission lines of CH_x radicals within the glow region. The dependence of the intensity ratio $I(CN)/I(N_2^*)$ on the current shows an increased content of CN radicals in comparison with N_2^* molecules, which is in good agreement with the increasing HCN concentration measured by FTIR analysis.

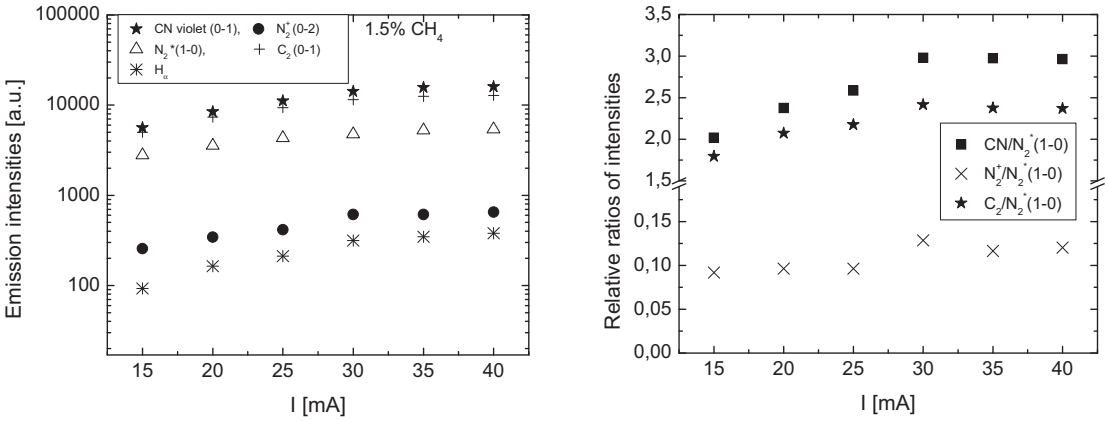

Fig. 5. Emission intensities and ratios for the selected emission bands in a gas mixture of 1.5% CH_4 in N_2.

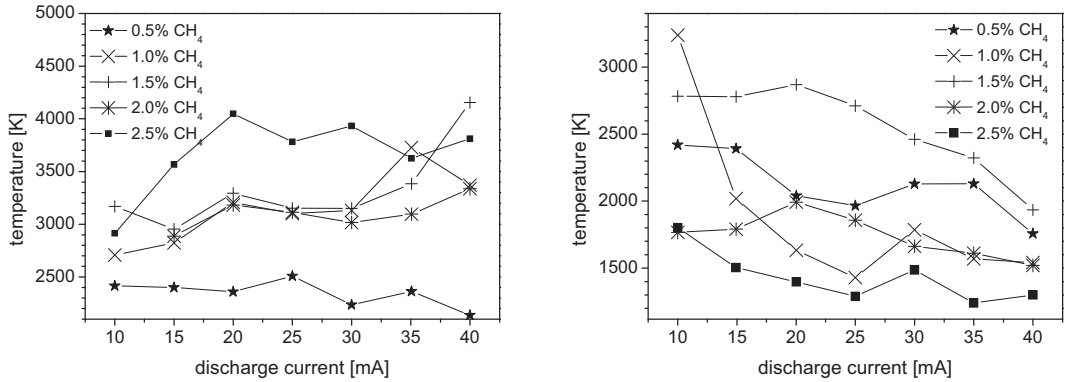

Fig. 6. Rotational temperatures calculated from the nitrogen second positive (left) and CN violet (right) 0–0 bands.

Since many emission bands of N_2 and CN overlap (Fig. 4) we have selected only regions where there is no overlap for the further detailed analysis and plasma parameters calculation. The CN violet 0–0 band was measured with high resolution (using 3600 g/mm grating and was used to make a rotational temperature calculation by adopting the classical pyrometric line procedure using rotational lines $J = 3$, 4, 7–16 and the rotational constants given by Prasad et al. [26]. The LifBase software [27] was used for the rotational lines assignment. The same procedure was applied for neutral nitrogen in N_2 ($C^3\Pi_u$) state rotational temperature calculation. In this case, the spectrum of 0–0 nitrogen second positive band (rotational lines with $J = 40$–50) was measured using the 1200 g/mm grating. The line assignment was made with SpecAir software [28] using rotational constants given in [29].

The rotational temperatures calculated using both methods are shown in Figure 6. The N_2 rotational temperature is more or less discharge current independent only slightly increasing with the increase of methane concentration in the gas mixture. On the other hand, the CN rotational temperature decreased with increasing current in range from 3200 to 1200 K. The maximum CN rotational temperature was obtained in the nitrogen with 1.5% of methane, no clear temperature dependence on methane concentration was found. The experimental uncertainty for both temperatures is about 300 K.

Table 1. Bands used for the vibrational temperature calculations.

Spectral system	Used band heads	Molecular constants from
N_2 1st neg.	0–2; 1–3; 2–4; 3–5	[29]
N_2 2nd pos.	1–0; 2–1; 3–2	[29]
CN violet	0–1; 1–2; 2–3; 3–4; 4–5	[30]
C_2 Swan	0–1; 1–2; 2–3; 3–4	[31]

Vibrational temperatures were calculated from nitrogen, CN and C_2 spectra. The spectral bands used and their associated molecular constants are given in Table 1. Only non overlapping sequences with signal/noise ratio better than 5 were used for these calculations. The average uncertainties in the calculated values was between 10 and 15%. Bands of –1 sequence of nitrogen second positive and +2 sequence of nitrogen first negative systems were applied with using transition constants (wavelength and transition probability) given in [29]. In the case of CN, spectra of +1 sequence with constants given by [30] were used. Constants given by [31] were used with intensities of –1 sequence for the C_2 molecule vibrational temperature calculation.

The electron temperature was not calculated because intensity of H^β line was too low and it was significantly overlapped by C_2 Swan bands, too.

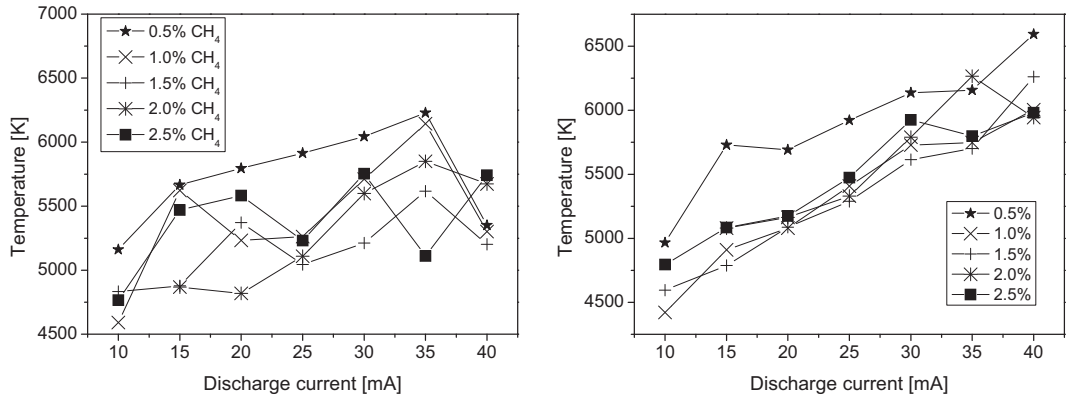

Fig. 7. Dependence of N_2^+ and CN vibrational temperatures on the discharge current for various CH_4 content.

The vibrational temperature (4800–6200 K) of the N_2^+ ion is found to decrease with increasing CH_4 content and increased with the discharge current until it showed a rapid fall at 40 mA (Fig. 7). The plasma power and CH_4 molar ratio have a significant effect on the CN vibrational temperature, with values from 4200 to 6500 K and was directly proportional to the current (Fig. 7). The vibrational temperature of the nitrogen C state increased both with methane content and applied energy. The vibrational temperature of carbon diatomic molecule increased both with carbon content and applied power (Fig. 8). It should be noted that the data obtained for 2.0% methane in a nitrogen mixture was significantly different from the other data.

3.3 Determination of the electron density and specific input energy

Using the simplified relation:

$$j = \frac{I}{\frac{1}{4}\pi\Phi^2}, \tag{3}$$

it was possible to estimate the current density within an order of magnitude. It should once again be noted that the plasma was not gliding due to the low gas flow rate, just the electrode configuration was similar to that of gliding arc; a stable glow plasma channel occurred at the shortest electrode distance only! Therefore, the electric field did not vary along the glow sheet.

The typical glow plasma channel in CH_4/N_2 gas mixture at discharge current $I = 15$ mA has a diameter $\Phi = 1$ mm and length 2 mm, $j = 1.9$ A/cm^2. The electron number density n_e is a very important parameter in characterizing the plasma and can be derived from the measured current density and reduced electric field E/N, when N is the gas density for given T. The simplest estimate of n_e can be then obtained using the expression for the current density:

$$j = en_e v_d, \tag{4}$$

where e is the elementary charge and v_d is the electron drift velocity. The electron drift velocity is given by the electron mobility μ_e and the electric field strength E:

$$v_d = \mu_e E, \tag{5}$$

where E was approximately measured from the applied voltage (400 V) and the plasma column length (2 mm). The reduced electron mobility $\mu_e p$ can be considered constant in our experimental conditions i.e. $\mu_e p = 5.87 \times 10^7$ cm^2 Pa V^{-1} s^{-1} [32]. The pressure should be better represented by the gas density N to accommodate for the elevated gas temperatures T_g (to $T_r \sim T_g \sim 2700$–3700 K) at $p = 101$ kPa atm, similar to representing the reduced field as E/N rather than E/p. In N-representation, $\mu_e N$ reached values in range from 1.2×10^{22} to 7.8×10^{22} cm^{-1} V^{-1} s^{-1}. This value could be then used in the expression of the electron drift velocity and the electron density can be calculated [33]:

$$n_e = \frac{j}{e\mu_e N\frac{E}{N}}. \tag{6}$$

Such that n_e was estimated to be of the order of $\sim 10^{13}$ cm^{-3}. With increasing current the electron density increased resulting in a more conductive plasma, which was confirmed by the observation of a slight decrease in the applied voltage and an increase in the ion signal.

4 Discussion of experimental results

4.1 Plasma processes – First steps leading to an organic chemistry

Within a CH_4/N_2 plasma discharge, electron-molecule interactions dominate leading to the formation of a large number of chemically reactive species. For example the two lowest excited singlet states $CH_4(S_1)$ (9.6 eV) and $CH_4(S_2)$ (11.7 eV), formed in electron-methane collisions rapidly dissociate into radicals such as CH_3, CH_2, CH, C [34]:

$$\mathrm{e}\,(\varepsilon > 10\ \mathrm{eV}) + \mathrm{CH_4} \rightarrow \mathrm{CH_4}\,(\mathrm{S_1}, \mathrm{S_2}) + \mathrm{e} \tag{7}$$

$$\mathrm{CH_4}\,(\mathrm{S_1}, \mathrm{S_2}) \rightarrow \mathrm{CH_3} + \mathrm{H} \tag{8a}$$

$$\mathrm{CH_2} + \mathrm{H} + \mathrm{H} \tag{8b}$$

$$\mathrm{CH_2} + \mathrm{H_2} \tag{8c}$$

$$\mathrm{CH} + \mathrm{H_2} + \mathrm{H}. \tag{8d}$$

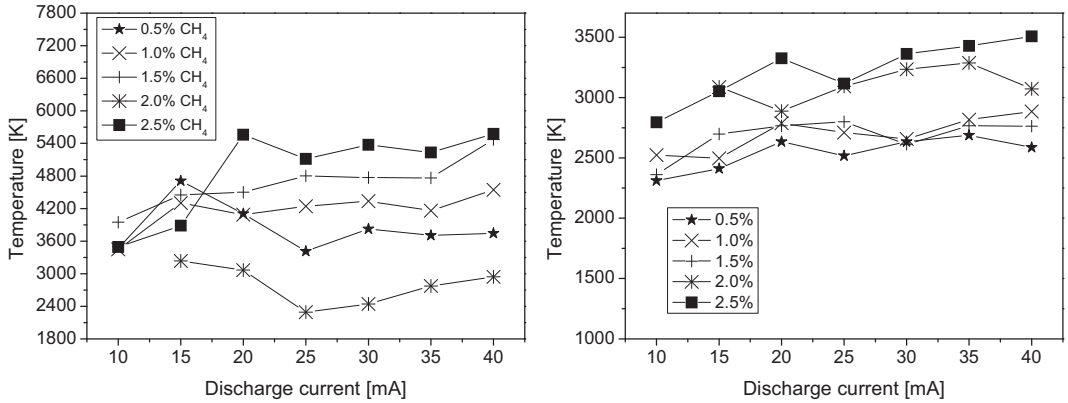

Fig. 8. Vibrational temperatures calculated from the nitrogen second positive $\Delta v = -1$ sequence (left) and C_2 Swan system $\Delta v = +1$ sequence (right).

If the electron energy is higher than 12.75 eV, ionization of CH_4 occurs in the discharge [10,35,36]:

$$\mathrm{e}\,(12.75\ \mathrm{eV}) + \mathrm{CH_4} \rightarrow \mathrm{CH_4^+} + 2\mathrm{e} \tag{9}$$

$$\mathrm{e}\,(14.3\ \mathrm{eV}) + \mathrm{CH_4} \rightarrow \mathrm{CH_3^+} + \mathrm{H} + 2\mathrm{e} \tag{10}$$

$$\mathrm{e}\,(15.1\ \mathrm{eV}) + \mathrm{CH_4} \rightarrow \mathrm{CH_2^+} + \mathrm{H_2} + 2\mathrm{e} \tag{11}$$

$$\mathrm{e} + \mathrm{CH_4} \rightarrow \mathrm{H^+} + \mathrm{CH_3} + 2\mathrm{e} \tag{12}$$

$$\mathrm{e}\,(22.2\ \mathrm{eV}) + \mathrm{CH_4} \rightarrow \mathrm{CH^+} + \mathrm{H} + \mathrm{H_2} + 2\mathrm{e} \tag{13}$$

$$\mathrm{e} + \mathrm{CH_4} \rightarrow \mathrm{H_2^+} + \mathrm{CH_2} + 2\mathrm{e} \tag{14}$$

$$\mathrm{e}\,(25\ \mathrm{eV}) + \mathrm{CH_4} \rightarrow \mathrm{C^+} + 2\mathrm{H_2} + 2\mathrm{e}. \tag{15}$$

Since bands of excited and ionic nitrogen are dominant and lines of atomic nitrogen were also observed in the OES spectra, electron impact ionization and dissociation of N_2 molecule clearly also has a significant role in the reaction kinetics [34]:

$$\mathrm{N_2}\left(\mathrm{X}^1\Sigma_g^+\right) + \mathrm{e}\,(11.1\ \mathrm{eV}) \rightarrow \mathrm{N_2}\left(\mathrm{C}^3\Pi_u^+\right) + 2\mathrm{e} \tag{16}$$

$$\mathrm{N_2}\left(\mathrm{X}^1\Sigma_g^+\right) + \mathrm{e}\,(15.63\ \mathrm{eV}) \rightarrow \mathrm{N_2^+}\left(\mathrm{X}^2\Sigma_g^+\right) + 2\mathrm{e} \tag{17}$$

$$\mathrm{N_2}\left(\mathrm{X}^1\Sigma_g^+\right) + \mathrm{e}\,(16.84\ \mathrm{eV}) \rightarrow \mathrm{N_2^+}\left(\mathrm{A}^2\Pi_u\right) + 2\mathrm{e} \tag{18}$$

$$\mathrm{N_2}\left(\mathrm{X}^1\Sigma_g^+\right) + \mathrm{e}\,(18.76\ \mathrm{eV}) \rightarrow \mathrm{N_2^+}\left(\mathrm{B}^2\Sigma_u^+\right) + 2\mathrm{e} \tag{19}$$

$$\mathrm{N_2}\left(\mathrm{X}^1\Sigma_g^+\right) + \mathrm{e}\,(23.53\ \mathrm{eV}) \rightarrow \mathrm{N_2^+}\left(\mathrm{C}^2\Sigma_g^+\right) + 2\mathrm{e} \tag{20}$$

$$\mathrm{N_2}\left(\mathrm{X}^1\Sigma_g^+\right) + \mathrm{e}\,(26.66\ \mathrm{eV}) \rightarrow \mathrm{N^+}\left(^3\mathrm{P}\right) + \mathrm{N}\left(^2\mathrm{D}\right) + 2\mathrm{e} \tag{21a}$$

$$\mathrm{N_2}\left(\mathrm{A}^3\Sigma_u^+, \mathrm{a}^1\Pi_g, \mathrm{a'}^1\Sigma_u^-\right) + \mathrm{e} \rightarrow \mathrm{N^+}\left(^3\mathrm{P}\right) + \mathrm{N}\left(^2\mathrm{D}\right) + 2\mathrm{e}. \tag{21b}$$

The population of N_2 ($C^3\Pi_u$) states (upper level of the detected second positive system) is mainly due to direct electron impact excitation from the ground state $X^1\Sigma_g^+$ [37,38], which is a result of the collision with electrons via reaction (16), whose energy is above the excitation threshold (11.1 eV). Reaction (19) is responsible for the electron impact excitation of N_2 molecule from ground state to N_2^+ ($B^2\Sigma_u$) excited state, which is the upper level of the detected first negative system. The measured spectra also contain a weak line of N^+ ion, which either suggests that the discharge contains energetic electrons with energies up to 26 eV (reaction (21a)) or N^+ is generated by stepwise processes via nitrogen metastables (reaction (21b)). Note, usually in atmospheric pressure discharges direct electron impact processes of high energy threshold are less important but in our case due to a high intensity of local electric field near the shaped electrode surface they must be taken into the account. Moreover, excited states of N_2 can also induce CH_4 dissociation into its lower radicals [10,39]. Thus electrons are the primary initiators of the organic chemistry induced by the discharge.

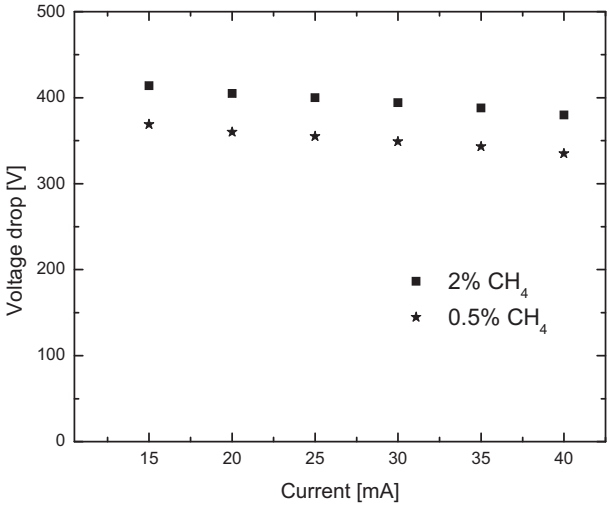

Fig. 9. Current-voltage characteristics in CH_4/N_2 plasma for 0.5 and 2% CH_4 content.

4.2 Processes leading to the synthesis of the observed HCN, C_2H_2 and NH_3

The formation of the observed products HCN, C_2H_2, and NH_3 is assigned to a complex plasma-chemistry.

Therefore, here we will discuss only the most important reaction channels with the highest reaction rates leading to the observed organic chemistry, which occur after the aforementioned electron induced CH_4 dissociation and N_2 excitation/ionization channels.

Atomic N and CH_2/CH_3 radicals, play an important role in the production of the detected HCN. Its formation can be direct (reactions (22) and (23)) [10,35,39] or/and indirect by a two-step process (24)–(25) through a highly unstable intermediate product, H_2CN [10,39]:

$$N + CH_3 \rightarrow HCN + H_2 \quad (22)$$

$$N + CH_2 \rightarrow HCN + H \quad (23)$$

$$N + CH_3 \rightarrow H_2CN + H \quad (24)$$

$$N + H_2CN \rightarrow HCN + NH \quad (25)$$

$$N + CH_2 \rightarrow CN + H_2 \quad (26)$$

$$CN + CH_4 \rightarrow HCN + CH_3. \quad (27)$$

In our case a faster, two-step process (26)–(27) is assumed to be a most possible source of HCN due to a high concentration of CN radicals measured by OES analysis. This assumption is in good accordance with experimental data which show an increasing HCN concentration with increasing intensity of CN violet system?

However, due to the absence of CH radicals in the glow region (lack of CH bands in the OES spectra), the reaction of CH_x radicals are assumed to be likely in the afterglow/recombination zone and most of the HCN formation is assumed to be due to reactions of primary CN radicals from the glow region with CH_4.

Because no C_2H_6 was observed during the measurements and C_2H_6 is expected to be predominantly formed by reactions of CH_3 radicals with each other, reactions (24) and (25) and other CH_3-depended processes can be neglected due to the lack and high instability of CH_3 radicals, which are possibly dissociated to lower radicals by high energy electrons. Note the mutual collision frequency of CH_3 radicals is much lower ($\sim$3–4 orders of magnitude) than collision frequency of CH_3 with other species.

C_2H_2, as the only stable hydrocarbon detected by ex-situ FTIR analysis, can possibly be formed by reactions of reactive C, CH and CH_2 radicals via the one-step (reaction (28)) or/and two-step processes (29)–(30). Reaction (29) is supported by our experimental results since the intensity of carbon lines increases with increasing C_2H_2 concentration, furthermore, the total dissociation of CH_4 to C atoms is verified with a brownish-black deposit observed at the electrodes. Unfortunately, surface analysis of this deposit could not be made due to technical reasons. The fast consummation of CH_2 radicals within the plasma could explain the lack of expected C_2H_4 in our FTIR spectra. Since emission lines of CH radicals were not present in the OES spectra and only H, C lines and C_2 Swan bands have been detected in the glow region, we can assume that reactions leading to C_2H_2 production only occur in the afterglow and recombination zones of the discharge reactor where energetic electrons are no longer present and excited states play the role of energy reservoirs.

$$CH + CH \rightarrow C_2H_2 \quad (28)$$

$$CH_2 + C \rightarrow H + C_2H \quad (29)$$

$$CH_2 + C_2H \rightarrow CH + C_2H_2. \quad (30)$$

NH_3 is produced in several steps, first CH_4 and its radicals react with N_2^+ to form NH radicals in the glow region, described by reactions (31) and (32) [18,19,34,40]. These reactions are probably the major route due to their highest rate constant [34]. N atoms adhered to the electrodes may also react with any free hydrogen to form NH radicals [18,19,40]. These NH radicals can then form NH_3 in the afterglow region via reaction (33) [34,40]. Note, process (33) is a catalytic reaction therefore NH_3 synthesis is probable predominant near the electrode surface in the afterglow region where it is not dissociated by the active heavy species or by electron collisions. This is the reason, why could not detect NH lines in the emission spectra. Since electrons are mainly consumed in CH_4 dissociation and N_2 excitation, only a smaller part can contribute in reaction (32), leading to a low NH_3 concentration measured.

$$N_2^+ + CH_4 \rightarrow N_2H^+ + CH_3 \quad (31)$$

$$N_2H^+ + e \rightarrow NH + N \quad (32)$$

$$NH + H_2 \rightarrow NH_3. \quad (33)$$

It should be noted that FTIR spectra of the gaseous mixture did not indicate the presence of any other stable carbon-nitrogen compounds in the gaseous phase. The major part of the plasma chemistry is expected to occur in the glow region where active radicals and ions are present. However the radical products may also undergo heterogeneous reactions between the electrode surfaces and the gas, not to mention the homogeneous reactions in the afterglow and recombination zone, where active radicals and metastables of nitrogen with long lifetimes play an important role. A brown deposit (composed from C_xN_y, $x \approx y$) was observed on the knife electrodes and the outlet holes due to the increasing content of C radicals but none was observed on the KCl windows in the measurement cell. These observations led us to consider the hypothesis that such a deposition is due to charged particles moving in the discharge electrode gap causing a set of homogeneous (in the active discharge volume) and heterogeneous (plasma catalyst on the electrode surface) reactions creating soot/deposit formation. In other words, only a small amount of the solid particles produced escape from the discharge reactor. This deposit is most likely formed from nitrogen compounds, especially CN which is also known as a precursor of polymer films and aerosols [15–17]. The most likely primary processes leading to the polymer formation is a transport of active CN and C/C_2 radicals onto the electrode surfaces where they are neutralized before undergoing a series of homogeneous reactions with other radicals leading to deposit formation. Moreover, it is postulated that negative ions may play a key role in the formation of such deposits [23].

4.3 Influence of the initial CH_4 content and specific input energy on the NH_3 and HCN formation

The concentration of most of the detected products was found to increase with increasing CH_4 content. For example NH_3 concentrations increased with increasing CH_4 content until it reached values between 200 and 350 ppm while HCN concentrations increased up to 1250 ppm proportionally to additional CH_4. This phenomena can be explained by the high density of active CN radicals within the glow region which consume the missing H atoms to produce HCN faster than stepwise reaction channels of NH_3 formation in the recombination zone. The rising density of these products can also be explained by the increasing density of electrons as in equation (6).

Because we could not measure the electron temperature T_e directly due to low H^β line intensity and non-equilibrium conditions in the plasma we can not accurately estimate the reaction branching ratios and the relative of importance of electrons and excited/charged nitrogen molecules in the formation of organic products. However, the absence of larger hydrocarbons indicates that, in our discharge conditions, the radicals of CH_4 are more reactive with nitrogen than with themselves, thus resulting higher contribution in N-reach product formation.

5 Conclusions

In this paper we present the results of both a FTIR and OES study of the gaseous products and radicals formed in a glow discharge fed by four different atmospheric pressure mixtures of N_2:CH_4 (0.5, 1, 1.5 and 2% CH_4) operated in a flowing regime at different discharge currents (from 15 up to 40 mA). FTIR analysis of the gaseous products showed that HCN, C_2H_2, NH_3 are the main products of our CH_4/N_2 abnormal glow plasma. The yields of these compounds are such that HCN > NH_3 > C_2H_2. The discharge current has a significant effect on the product synthesis and electron density. The continuous glow discharge was "hot" with T_g reaching 3200 K, since most of electron energy is converted into gas heating. The plasma was close to LTE but not close enough to assume a Maxwell distribution. Using our OES study we could estimate temperatures T_r and T_v which – together with the electrical parameters – allowed us to calculate the current and electron number densities in the discharge with typical values of 1.9–5.1 A/cm^2 and $n_e \sim 10^{13}$ cm^{-3}.

Such experiments can provide information that can aid our understanding of processes in Titan's atmosphere. Within the discharge we observed the formation of the same compounds as observed in Titan's atmosphere by the Huygens surface package and by Cassini Observer. Furthermore discharges can provide relevant information on the formation of the anions [1] and have therefore allowed of the anions observed by Cassini to be identified. However, we note that different discharges have different sources of ions/excited molecules and thus when using discharges as a simulation mimic it is necessary to carefully define the plasma conditions and their relevance to specific regions of Titan's atmosphere.

This research project was supported by the Slovak Grant Agency, Slovak Research and Development Agency, Grant UK/381/2009 and UK/389/2008, VEGA 1/0051/08, project SK-CN-0029-07, APVV 0365-07, ESF COST Actions CM0601, CM0805 and EIPAM, EUROPLANET TNA2 programme and Research plan of Czech Ministry of Education No. MSM0021630501.

References

1. V. Vuitton, P. Lavvas, R.V. Yelle, M. Galand, A. Wellbrock, G.R. Lewis, A.J. Coates, J.-E. Wahlund, Planet. Space Sci. **57**, 1558 (2009)
2. S. Vinatier et al., Icarus **188**, 120 (2007)
3. G.J. Molina-Cuberos, J.J. López-Moreno, R. Rodrigo, Geophys. Res. Lett. **27**, 1351 (2000)
4. E.L.O. Bakes, C.P. McKay, C.W. Bauschlicher, Icarus **157**, 464 (2002)
5. A.J. Coates, F.J. Crary, G.R. Lewis, D.T. Young, J.H. Waite, E.C. Sittler, Geophys. Res. Lett. **34**, L22103 (2007)
6. J.H. Waite, D.T. Young, T.E. Cravens, A.J. Coates, F.J. Crary, B. Magee, J. Westlake, Science **316**, 870 (2007)
7. V. Vuitton, R.V. Yelle, P. Lavvas, Phil. Trans. R. Soc. A (2009), doi:10.1098/rsta.2008.0233
8. J.M. Bernard, E. Quirico, O. Brissaud, G. Montagnac, B. Reynard, P. McMillan, P. Coll, M.J. Nguyen, F. Raulin, B. Schmitt, Icarus **185**, 301 (2006)
9. C.D. Pintassilgo, J. Loureiro, G. Cernogora, M. Touzeau, Plasma Sources Sci. Technol. **8**, 463 (1999)
10. C. Szopa, G. Cernogora, L. Boufendi, J. Correia, P. Coll, Planet. Space Sci. **54**, 394 (2006)
11. H. Imanaka, B.N. Khare, J.E. Elsila, E.L.O. Bakes, C.P. McKay, D.P. Cruikshank, S. Sugita, T. Matsui, R.N. Zare, Icarus **168**, 344 (2004)
12. Y. Sekine, H. Imanaka, T. Matsui, B.N. Khare, E.L.O. Bakes, C.P. McKay, S. Sugita, Icarus **194**, 186 (2008)
13. P. Coll, D. Coscia, M.C. Gazeau, E. de Vanssay, J.C. Guillemin, F. Raulin, Adv. Space Res. **16**, 93 (1995)
14. C. Ponnamperuma, F. Woeller, Nature **203**, 272 (1964)
15. R.N. Gonzalez, S.I. Ramirez, Adv. Space Res. **19**, 1121 (1997)
16. R.N. Gonzalez, S.I. Ramirez, J.G. de la Rosa, P. Coll, F. Raulin, Adv. Space Res. **27**, 271 (2001)
17. S.I. Ramirez, R.N. Gonzalez, P. Coll, F. Raulin, Adv. Space Res. **36**, 274 (2005)
18. J.M. Bernard, P. Coll, A. Coustenis, F. Raulin, Planet. Space Sci. **51**, 1003 (2003)
19. K. Plankensteiner, H. Reiner, B.M. Rode, T. Mikoviny, A. Wisthaler, A. Hansel, T.D. Mark, G. Fischer, H. Lammer, H.O. Rucker, Icarus **187**, 616 (2007)
20. A. Indarto, J.-W. Choi, H. Lee, H.K. Song, Energy **31**, 2986 (2006)
21. M. Młotek, J. Sentek, K. Krawczyk, K. Schmidt-Szałowski, Appl. Catal. A: Gen. **366**, 232 (2009)
22. http://www.cfa.harvard.edu/hitran
23. G. Horvath, J.D. Skalny, N.J. Mason, M. Klas, M. Zahoran, R. Vladoiu, M. Manole, Plasma Sources Sci. Technol. **18**, 034016 (2009)
24. M.A. Hafez, M.A. Khedr, F.F. Elaksher, Y.E. Gamal, Plasma Sources Sci. Technol. **12**, 185 (2003)
25. A. Bogaerts, J. Anal. At. Spectrom. **14**, 1375 (1999)

26. C.V.V. Prasad, P.F. Bernath, C. Frum, Engleman, J. Mol. Spectrosc. **151**, 459 (1992)
27. J. Luque, D.R. Crosley, LIFBASE: Database and Spectral Simulation Program (Version 1.5), SRI International Report MP 99-009, 1999
28. Specair Version 2.1, `http://www.specairradiation.net`
29. F.R. Gilmore, R.R. Laher, P.J. Espy, J. Phys. Chem. Ref. Data **21**, 1005 (1992)
30. C.O. Laux, Radiation Nonequilibrium Collisional-Radiative Models, von Karman Institute Lecture Series 2002-07, *Physico-Chemical Modeling of High Enthalpy and Plasma Flows*, edited by D. Fletcher, J.-M. Charbonnier, G.S.R. Sarma, T. Magin (Rhode-Saint-Genèse, Belgium, 2002)
31. R.B. King, Astrophys. J. **108**, 429 (1948)
32. Yu.P. Raizer, *Gas Discharge Physics* (Springer, New York, 1991)
33. Z. Machala, M. Janda, K. Hensel, I. Jedlovsky, L. Lestinska, V. Foltin, V. Martisovits, M. Morvova, J. Mol. Spectrosc. **243**, 194 (2007)
34. M. Bai, Z. Zhang, X. Bai, H. Gao, Plasma Chem. Plasma Process **15**, 87
35. J. Loureiro, A. Ricard, J. Phys. D: Appl. Phys. **26**, 163 (1993)
36. J. Loureiro, C.M. Ferreira, J. Phys. D: Appl. Phys. **22**, 1680 (1989)
37. Z.Lj. Petrovic, P. Tochikubo, S. Kakut, T. Makabe, J. Appl. Phys. **73**, 2163 (1993)
38. F. Debal, M. Wautelet, J. Bretagne, J.P. Dauchot, M. Hecq, Plasma Sources Sci. Technol. **9**, 1 (2000)
39. Y.L. Yung, M. Allen, J.P. Pinto, Astrophys. J. Suppl. Ser. **55**, 465 (1984)
40. M. Bai, Z.T. Zhang, X. Bai, N. Wang, IEEE Trans. Plasma Sci. **31**, 1285 (2003)